The Cryosphere Discuss., 5, 3627–3660, 2011
www.the-cryosphere-discuss.net/5/3627/2011/
doi:10.5194/tcd-5-3627-2011

The Cryosphere Discussions

Stable isotope and gas properties of two ice wedges from Cape Mamontov Klyk, Laptev Sea, Northern Siberia

T. Boereboom[1], D. Samyn[1,*], H. Meyer[2], and J.-L. Tison[1]

[1]Laboratoire de Glaciologie, Université Libre de Bruxelles, Belgium
[2]Alfred Wegener Institute for Polar and Marine Research, Research Unit Potsdam, Potsdam, Germany
[*]now at: Dept. of Mechanical Engineering, Nagaoka University of Technology, Nagaoka, Japan

Received: 30 November 2011 – Accepted: 10 December 2011
– Published: 21 December 2011

Correspondence to: T. Boereboom (thierry.boereboom@ulb.ac.be)

Published by Copernicus Publications on behalf of the European Geosciences Union.

Abstract

This paper presents and discusses the texture, fabric and gas properties (contents of total gas, O_2, N_2, CO_2, and CH_4) of two ice wedges from Cape Mamontov Klyk, Laptev Sea, Northern Siberia. The two ice wedges display contrasting structures: one being of relatively "clean" ice and the other showing clean ice at its centre as well as debris-rich ice on its sides (referred to as ice-sand wedge). A comparison of gas properties, crystal size, fabrics and stable isotope data ($\delta^{18}O$ and δD) allows discriminating between three different facies of ice with specific paleoenvironmental signatures, suggesting different climatic conditions and rates of biological activity. More specifically, total gas content and composition reveal variable intensities of meltwater infiltration and show the impact of biological processes with contrasting contributions from anaerobic and aerobic conditions. Stable isotope data are shown to be valid for discussing changes in paleoenvironmental conditions and/or decipher different sources for the snow feeding into the ice wedges with time. Our data also give support to the previous assumption that the composite ice wedge was formed in Pleistocene and the ice wedge in Holocene times. This study sheds more light on the conditions of ice wedge growth under changing environmental conditions.

1 Introduction

There is growing evidence that the permafrost environment has been changing recently (Brown and Romanovsky, 2008; IPCC, 2007; Wagner and Liebner, 2009). This points to the urgent need to study permafrost and its main physical and biogeochemical properties in order to follow the transformations of this widespread ecosystem and to quantify its contribution to the global greenhouse effect. The periglacial environment has become increasingly wet and the depth of the permafrost table has increased in the last decades (Brown and Romanovsky, 2008; Kolchugina and Vinson, 1993; Nelson and Anisimov, 1993). This increase of water in the liquid state is thought to stimulate

TCD
5, 3627–3660, 2011

methane production which is a greenhouse gas 23 times more effective than carbon dioxide (e.g. Lambert et al., 2006).

Studies of ice properties within ice wedges are a rich source of information in several aspects: facies, texture and fabric studies provide details on genetic processes (Black, 1954, 1978, 1963; Corte, 1962; Shumskii, 1964; Gell, 1976, 1978a, b; Samyn et al., 2005) while stable water isotopes (δ^{18}O and δD) additionally reveal information about paleotemperatures and paleoenvironmental conditions since ice wedges are built from both the winter snow and the spring meltwater (Meyer et al., 2002a, b; Lauriol et al., 1995; Vasil'chuk and Vasil'chuk, 1998; Vaikmäe, 1989; Dereviagin et al., 2002; Raffi et al., 2004), provided fractionation processes from phase changes are discussed and secondary processes shown to be limited.

In this paper, we propose a multi-parameter approach using stable isotope composition, total gas content, gas composition, texture and fabric of two ice wedges from the Laptev Sea coast. The sampling was carried out in the frame of the research project "Process studies of permafrost dynamics in the Laptev Sea", which addressed the paleoenvironmental history of the Cape Mamontov Klyk area (Bobrov et al., 2009; Schirrmeister et al., 2008). We use total gas content and gas composition measurements as a tool to describe the various physical and biological processes involved in ice-wedge genesis and the prevailing environmental conditions. We combine those results to a co-isotopic analysis (δD vs. δ^{18}O) of the samples to show that δ- and deuterium excess (d) values of our ice wedges can be interpreted in terms of contrasting paleoclimatic and paleoenvironmental conditions between the Pleistocene and the Holocene.

2 Study area and ice wedge description

The two studied ice wedges are part of an outcrop on the Laptev Sea coast, about 300 km west from the Lena Delta (73°36′ N; 117°10′ E, Fig. 1). This area belongs to the subarctic tundra in a region of continuous permafrost, with a thickness of 400–600 m

TCD
5, 3627–3660, 2011

(Yershov, 1989). The active layer shows a maximum thaw depth of 0.2–0.5 m in July. The area is dominated by a continental arctic climate with long severe winters and short cold summers.

The cliff from which the ice wedges originate is subdivided into four different sedimentological units (A to D, from old to young) and described in detail by Schirrmeister et al. (2008) and Bobrov et al. (2009). From the bottom of the cliff to its summit, we distinguish a lower sand unit (unit A) that consists of yellowish-grey, irregularly-laminated fine-grained sand, lacking visible plant remains. Above, unit B consists of an alternation of four cryoturbated peat-rich horizons and irregularly-laminated, dark-grey silty to fine-grained sandy interbeds. Unit C is the Ice Complex that is a type of ice-rich permafrost deposit of Late Pleistocene age widespread in Arctic Siberia. The Ice Complex deposits are composed of alternating mineral-rich (greyish) and organic-rich (brownish) sediment layers. The upper unit (unit D) consist of peat soils of Holocene age originating from fillings of small thermokarst or polygonal ponds developed on top of the Ice Complex or from Holocene thermoerosional or fluvial deposits.

Ice wedge 26 (IW-26, Fig. 2a) was sampled within unit C in the upper part of the cliff, at 18.6 m above sea level, and is therefore embedded within the Pleistocene Ice Complex sediments (Bobrov et al., 2009; Schirrmeister et al., 2008). IW-26 is only 1.6 m in width and about 2.5 m in height. Sampling was performed across the full ice-wedge width and approximately 1.2 m below the surface. The sample consists of foliated grey to white, and in parts yellowish, ice with small gas bubbles (millimetric). The wedge ice shows a low content of mineral particles and organic matter (fine-disperse individual particles or thin layers following the foliation).

The second ice wedge studied in this paper, IW-28 (Fig. 2b), has been attributed to unit A in the lower part of the cliff and was sampled at 1 m above sea level. It developed in sandy sediments. IW-28 is up to 5 m wide in its upper part. The ice wedge is laterally associated with an ice-sand wedge (ISW-28), a portion of which was also sampled (Fig. 2b, left of sampling box). In the central section, the wedge ice has a white and milky appearance, and small millimetric gas bubbles are frequent (Fig. 4d). The mineral

TCD
5, 3627–3660, 2011

content and the organic matter contents are both low, with particles dispersion similar to that in IW-26 and foliation layers that are 1–3 mm wide. For the ice-sand wedge portion, the ice is mixed with a significant amount of fine-grained sediments alternating with clean ice layers.

3 Sampling and analytical methods

The ice wedges were sampled as ice blocks using a chain saw, in horizontal transects covering the entire ice-wedge width and partly including the ice-sand wedge section from now on referred to as ISW-28 (Fig. 2). Samples used in this paper for fabric, texture, gas and stable isotope analyses derived from horizontal sections (±1.5 cm thickness) in the upper part of the blocks.

Horizontal thin sections were prepared using a traditional biological microtome (Leitz 1400) for the clean ice and a diamond-wire saw (Well 6234) for the debris-laden ice, following the standard procedures from Langway (1958) and Tison (1994), respectively.

Crystal-size determination was performed using two different techniques. The first was the mean linear intercept method developed by Pickering (1976). The number of grain boundaries ($\bar{N}$) crossed by a random linear traverse of length ($\bar{L}$) across the thin section was averaged over many traverses. The mean grain diameter ($\bar{d}$) was estimated using the following equation: $\bar{d} = \bar{N}/\bar{L}$. The second method, proposed by Jacka (1984), estimates the mean diameter by counting the number of entire crystals in a known area and assuming a circular cross-section following the equation $\bar{d} = \sqrt{4A/\pi N}$, where A is the area of thin section studied and N is the crystal count.

Stable water isotopes were measured with a Finnigan MAT Delta-S mass spectrometer at the Alfred Wegener Institute, Research Unit Potsdam using equilibration techniques. Hydrogen and oxygen isotope ratios are given as per mil difference relative to V-SMOW (‰, Vienna Standard Mean Ocean Water), with internal 1σ errors better than 0.8 ‰ and 0.1 ‰ for δD and δ^{18}O, respectively (Meyer et al., 2000).

TCD
5, 3627–3660, 2011

Gas inclusions entrapped in the ice were analysed for their total gas volume (27 samples) and gas composition (CO_2, O_2, N_2, and CH_4). Gas composition (CH_4 = 24 samples, other gases = 30 samples) was measured by gas chromatography (Interscience Trace GC) using an FID detector for CO_2 and CH_4 and a TCD detector for O_2 and N_2. Between 20 to 35 grams of sample were used for each measurement. For CO_2, O_2 and N_2, we used the dry-extraction technique described in Raynaud et al. (1982) and Barnola et al. (1983). For CH_4, we used the melting-refreezing procedure described in Raynaud et al. (1988) and Blunier et al. (1993). The levels of precision of the measurements were 2.5 % for CO_2, 0.4 % for O_2 and N_2 and 3 % for CH_4. The total gas content (27 samples) was determined using a Toepler pump and a melting-refreezing extraction technique described in Martinerie et al. (1994). The precision of the measurements was ≤5 %.

The residual sediments collected after the gas analyses have been treated by HCl (1 mol l^{-1}) and H_2O_2 (30 %) for qualitative detection of calcium carbonate or organic matter, respectively.

4 Results

4.1 Stable ^{18}O and ^{2}H isotopes

Ice wedge IW-26 shows $\delta^{18}O$ values ranging between −22.6 ‰ and −25.8 ‰ and δD values between −170 ‰ and −191 ‰, respectively (Fig. 3a). The IW-26 samples plot on a slope of 6.63 in the co-isotopic diagram (Fig. 3c, grey squares). The isotopic composition of ice wedge IW-28 is also shown in Fig. 3a and a clear distinction has to be made between the two different facies of the ice wedge: the ice-sand wedge (ISW-28) and the ice wedge itself (IW-28), both in terms of deuterium-excess ($d = \delta D - 8\delta^{18}O$; Dansgaard, 1964; Fig. 3b) and co-isotopic relationship (Fig. 3c). This distinction coincides with a clear visual boundary between the two facies. The ice-sand wedge displays $\delta^{18}O$ values between −29 ‰ and −30.9 ‰ and δD values between −230 ‰

TCD
5, 3627–3660, 2011

and −246 ‰. The samples show a low variability in d ($1\sigma = \pm 0.6$ ‰) with a mean value of 1.4 ‰, and they are aligned on a slope of 8.03 in the co-isotopic plot. For the ice wedge part, δ^{18}O and δD range between −29.4 ‰ and −31.9 ‰, and between −229 ‰ and −247 ‰, respectively. The d also shows a low variability ($1\sigma = \pm 0.7$ ‰) with a mean value of 7.5 ‰ and a slope of 7.44 is measured in the co-isotopic diagram. The transition zone has a δ^{18}O between −29.5 ‰ and −29.9 ‰, a δD between −223 ‰ and −237 ‰, and shows variable d values intermediate between the other two parts (Fig. 3c).

4.2 Ice texture and fabrics

Figure 4 shows thin section photographs that are typical of the three main facies encountered in the two studied ice wedges. In IW-26, the texture is homogeneous, lacking any significant elongation (Fig. 4a). The crystal diameter is ranging between 0.40 and 0.60 cm (Fig. 5) and c-axe orientations are concentrated in the horizontal plane with preferred orientation perpendicular to the foliation azimuth (Fig. 6a). The ISW-28 texture shows, within a matrix of relatively large equigranular grains, several monocrystalline layers of elongated crystals with a well-developed "ribbon structure", and crystal growth being geometrically associated to the fine debris layers that surround them, oriented parallel to the (subvertical) foliation plane (Fig. 4b). On Fig. 5, crystal diameter is ranging between 0.2 and 0.4 cm. In IW-28, the central part of the ice wedge shows an equigranular texture (Fig. 4c), with crystals smaller than in ISW-28 (0.1 to 0.2 cm, Fig. 5). Both ISW-28 (Fig. 6b) and IW-28 (Fig. 6c) show c-axes orientation patterns similar to IW-26, although the preferred orientation perpendicular to the foliation azimuth is less obvious for ISW-28 given the limited number of observations (due to larger grains).

TCD
5, 3627–3660, 2011

4.3 Gas properties

The contrast between the three facies (IW-26, ISW-28 and IW-28) is also evident from their gas properties (Fig. 7). Table 1 summarizes minimum, mean and maximum values observed for the 3 facies and compares them to atmospheric pre-industrial and present day values and to meteoric ice range in ice sheets. We highlight that total gas content in our ice wedges are lower than in ice resulting from simple snow compaction as in ice sheet and that the total gas content of IW-28 is higher than those of ISW-28 and IW-26. For CO_2, the total mixing ratios are clearly higher than the atmospheric concentrations, the highest values are observed in IW-26 (mean = 62 000 ppmV) and the ISW-28 shows lower values (mean = 3000 ppmV) than IW-28 (mean = 25 000 ppmV). On the contrary, CH_4 mixing ratios show lowest values for IW-26 with values in the same range of the atmospheric concentration (mean = 1 ppmV), high values for IW-28 (mean = 8 ppmV) and very high values for ISW-28 (mean = 55 ppmV). Oxygen shows values lower than the atmosphere with values around 10 % and nitrogen is slightly higher, balancing other constituents.

4.4 Sediments properties

Residual sediments collected from 4 ice samples have been treated by HCl and H_2O_2 (2 samples from ISW-28 and 2 samples from IW-28). The ISW-28 samples have strongly reacted with H_2O_2 while the IW-28 samples only showed a soft reaction. It can thus be argued that there is organic matter in the sediment. On the other hand, the HCl treatment did not show any detectable bubbling activity under the binocular for all sediment. Specimens supporting the hypothesis that carbonate contents are negligible within the sediment enclosed in the ice wedges.

TCD
5, 3627–3660, 2011

5 Discussion

5.1 Ice texture and fabrics

Crystal size and shape provide information about ice formation processes (e.g. Paterson, 1994). Ice wedge IW-26 is clearly younger than IW-28 as indicated by its stratigraphic location within the cliff. IW-26 does not show variations in crystal size from the centre to the border (Fig. 5). There are however some arguments in favour of such variations in IW-28 (note the V-shape of the curve to the right of the ice-sand wedge, Fig. 5). It is unlikely that the larger crystal size (e.g. in IW-26) predominantly results from seasonal deformation. Indeed, crystal size is fairly homogeneous throughout the ice wedge and there is no evidence of structural features (folds, shears planes, etc.) that would be generated by seasonal ice-wedge contraction. Finally, the absence of ongoing deformation is further supported by the horizontal c-axes orientations (Black, 1954, 1963, 1976; Corte, 1962; Gell, 1976) and the absence of strain shadow within individual crystals. This suggests that the primary controls on the crystal size in IW-26 are temperature and possibly increased water infiltration, which would be consistent with an ice wedge developed under Holocene conditions.

ISW-28 shows a peculiar "ribbon-like" structure embedded into a matrix of equigranular crystals. This type of structure resembles those found in the "stratified facies" found in basal glacier ice (Knight, 1999; Lawson, 2007; Samyn et al., 2005). In this environment, this mono-crystalline ice layer "sandwiched" between two fine debris layers was likely formed as a result of recrystallization in an environment of liquid water streaming, generally as a thin film, at the ice bedrock interface and refreezing on the lee side of bedrock irregularities. These observations suggest liquid water occurrence during the ice-sand wedge formation. Debris incorporation resulted from particular surface conditions and specific mineral and/or water supply such as an increased part of surface matter content, or a thinner snow cover. These conditions obviously existed during the early stages of IW-28 development. We therefore assume that ice in ISW-28 was formed within different environmental conditions than ice in IW-28. The crystals in the

TCD
5, 3627–3660, 2011

latter are smaller and show an equigranular texture; crystal growth mechanisms were therefore probably slower in this debris-poor ice, suggesting potentially colder ice.

5.2 Gas properties

Gases analyses (Fig. 7) further support the conclusions drawn from the ice texture description. All samples display a low total gas content (Fig. 7, row 1) in comparison with meteoric glacier ice formed under dry conditions. We hypothesize that these low values are due to liquid water infiltration during the ice wedge formation. Indeed, bubble density, geometry and distribution (Fig. 4d) suggest that the studied wedge ice originated from a mixture of snow and water filling thermal contraction cracks in variable amount, rather than solely from snow compaction. Especially since it has been observed that water standing in the apex (above the crack) enters the crack at once. That is also why the mean isotopic composition of recent ice wedges often corresponds to that of snow. In these conditions, total gas content should follow an inverse relation to the liquid water content. The liquid water contribution is apparently larger for IW-26 than for IW-28. This is consistent with a colder environment for IW-28 also confirmed by the isotopic composition. Another characteristic feature of ISW-28 is that its gas content is alternating between very low values, down to about 10 $ml_{air}\,kg_{ice}^{-1}$ (the lowest in this study), and values intermediary between those of IW-26 and IW-28. This is the expected signature for alternation of episodes of film water refreezing as "ribbon layers" (low total gas content) incorporating sediments at the beginning and at the end of the refreezing process (phases of interruption of film waterflow), with an equigranular matrix corresponding more to wet snow consolidation (higher total gas content). Another potential explanation would be that the ribbon layers are due to the freezing of a water body from the rim of the crack towards its centre and the associated entrainment of particles, ions and gas bubbles. However, this would result in bubbles inclusions elongated perpendicular to the freezing front direction which are not detected here.

All CO_2 mixing ratios are largely above the present day atmospheric value of 390 ppmV (Fig. 7, row 2). This indicates that the ice did not form through simple

TCD
5, 3627–3660, 2011

low temperature pressure-driven dry firnification process of snow enclosing the atmospheric gas composition. Previous studies of ice forming close to a bedrock environment have shown that this is very often the case, mainly because of either the presence of liquid water and/or significant biological activity living on the enclosed organic matter fraction (Souchez et al., 1995a). Theoretically, the high CO_2 solubility in water could raise the CO_2 mixing ratio in the dissolved phase up to about 20 000 ppmV (at 0 °C and 1 atmosphere, with limited effect of pressure and impurities). Freezing of a CO_2 saturated freshwater reservoir in a closed system could therefore display such high CO_2 values. There are however a number of other potential ways to further increase the CO_2 mixing ratio in our ice wedge ice such as diffusion-driven gas fractionation at the freezing front, CO_2 degassing on calcium carbonate precipitation, thermal trapping or biological respiration. Solutes segregation as observed ahead of a freezing front, rejection of impurities at the interface by ice growing in a water reservoir will set up a strong diffusion gradient in the adjacent liquid boundary layer. This could lead to a further increase of the mixing ratio of the least diffusive gas in the solution, as for instance CO_2 (Killawee et al., 1998). However, theoretically, this effect cannot increase the CO_2 concentration by a factor higher than the ratio of the CO_2 diffusion coefficient (DCO_2) to the air diffusion coefficient (Dair) in water; i.e. by a factor of about 1.6 (using typical values for DCO_2, DN_2, DO_2). This would increase the CO_2 mixing ratio to about 30 000 ppmV, provided that freezing process can be assimilated in this case to ice growing in a liquid interface. Killawee et al. (1998) have shown that unidirectional freezing of a supersaturated $CaCO_3$ solution leads to a strong CO_2 enrichment of the refrozen water due to the CO_2 degassing resulting from the carbonate precipitation. The lack of reaction of our ice wedge sediments to HCl attack however does not support the existence of significant amount of $CaCO_3$. Finally, biological respiration is also a likely candidate, given a similar behaviour of our samples compared to segregated ice (Cardyn et al., 2007).

The considerations above suggest that the CO_2 mixing ratio of IW-26 (40 000–100 000 ppmV) is dominated by biological respiration processes while IW-28 CO_2 levels

TCD
5, 3627–3660, 2011

could still be fully explained by physical processes alone (although biological processes cannot be excluded). Isotopic measurements of the ^{13}C of CO_2 or of the ^{18}O of the O_2 in our samples would further support this assessment (Cardyn et al., 2007; Souchez et al., 2006), but these data are currently not available. Interestingly though, the range of CO_2 values in the IW-26 ice wedge is similar to that observed in the basal ice of the GRIP ice core (up to 130 000 ppmV), where $\delta^{18}O_{air}$ values as low as −39 ‰ clearly indicate the occurrence of bacterial respiration processes (Souchez et al., 2006). Tison et al. (1998) and Souchez et al. (1995b), among others, demonstrated that the GRIP basal ice developed under climatically mild pre-ice sheet periglacial conditions. The latter are thus potentially similar to those surrounding our ice-wedge samples. Another approach would be to test for the conservation of the sum of O_2 and CO_2 concentration, given the stoichiometry of the respiration reaction, as suggested by Souchez et al. (1995a). However this approach is not valid in our case since a liquid water phase is present allowing most of the carbon dioxide produced by the respiration process to dissolve as HCO_3^- into the solution, at least at normal pH levels (Zeebe and Wolf-Gladrow, 2001). There is also a clear contrast between the CO_2 concentrations of most of the ISW-28 samples as compared to those of IW-28. This contrast could reflect differences in the ice-wedge formation process. The CO_2 levels close to maximum solubility in IW-28 suggest limited exchange with the atmosphere and the reverse is valid for ISW-28, as also demonstrated by the contrast in total gas content. This supports the hypothesis of a contrasting dynamic between the genesis of the ribbon facies of ISW-28, the geometry of which suggesting higher temperature allowing recrystallization and/or open-system growth from a running water film, and of the ice within the central part of ice wedge IW-28, which results from bulk refreezing of a mixture of snow and interstitial water.

Methane also displays strong contrasts between the three ice-wedges facies, with a general inverse relation to the CO_2 concentration (Fig. 7, row 2 and 3). While IW-26 concentrations range between pre-industrial and present day values, IW-28 and ISW-28 are by a respective factor of 10 to 100 higher suggesting in situ CH_4 production.

TCD
5, 3627–3660, 2011

Methane production implies an anaerobic environment for the methanogenic archaea to work efficiently (e.g. Wagner and Liebner, 2009). Although ice wedges can be a source of methane production, the range of methane content observed seems to be negligible in regard with other methane sources studied for the carbon budgets in permafrost area (IPCC, 2007). Apart from a few values close to atmospheric in ISW-28, the O_2 concentration fluctuates around 10 % (Fig. 7, row 4). It is only half the atmospheric O_2 mixing ratio and it is hard to tell if this value is the gaseous composition of the local environment (in the crack into the frozen soil) before the bubbles close off or if this value is the result of biogeochemical post-genetic processes. Whichever way, it does not imply a fully anaerobic environment. However, one must recall that the measurements were taken from ±35 g samples each containing a large number of millimetric bubbles. As already suggested for the GRIP basal ice (where both high CO_2 and high CH_4 values were measured in the same samples) and in other environments like soils and marine sediments (Souchez et al., 1995b), the mean O_2 concentration might well reflect a situation where some bubbles are depleted in oxygen and others have concentrations close to atmospheric levels. The bubbles can therefore provide contrasted closed system micro-environments in some cases favourable to aerobic respiration (high CO_2, low CH_4) and in others to bacterially mediated methanogenesis (high CH_4, low CO_2). Note that the contrast in this CO_2/CH_4 relation is mainly between ice wedges, rather than within a given ice wedge. Brouchkov and Fukuda (2002) also observed an inverse correlation between CH_4 and CO_2 in ice wedges. Their study reveals an important CH_4 mixing ratio variability (2 to 6000 ppmV), which they attributed to the contrasted vegetation cover, which, in their case, consist of a forest that increase methane production.

The methane concentration of the ice-sand wedge ISW-28 contrasts with the central part of IW-28 displaying highest CH_4 levels in the ice-sand wedge whereas anaerobic conditions are somewhat less pronounced. This could be the expression of a higher availability of organic substrates in the debris-rich ice-sand wedge. This hypothesis is supported by the obviously positive reaction of H_2O_2 with the residual sediments from

TCD
5, 3627–3660, 2011

ISW-28. From the above discussion it is clear that both environmental, physical and biological controls need to be taken into account to interpret the observed gas properties in ice wedges. As demonstrated by the comparison between IW-26 and IW-28, it is not always when the temperatures are warmer that the highest CH_4 concentration levels are observed. This is supported by an ice-wedge study of Meyer et al. (2010a) in Northern Alaska, where an ice-wedge component formed during the colder Younger Dryas displays higher methane concentrations as compared to an ice wedge section formed during the warmer Allerød. Thus, the availability of organic matter within the deposits (as in ISW-28) and in semi-closed system conditions might favour methanogenesis and limit CH_4 conversion to CO_2.

5.3 Links to the $\delta^{18}O$ – δD isotopic composition of ice wedges

Results from texture, fabric and gas analyses allow to differentiate three different facies within the two studies ice wedges (IW-26, ISW-28 and IW-28), which can be discussed in terms of the available stable isotope data.

The IW-26 displays least negative δD and $\delta^{18}O$ values, largest crystal sizes, lowest total gas contents and is embedded in the Ice Complex structure of Pleistocene age. However, the isotopic composition is coherent with Holocene age ice wedges ($\delta^{18}O$ around −24 to −25 ‰; Meyer et al., 2000, 2002a, b; Dereviagin et al., 2002; Schirrmeister et al., 2002; Popp et al., 2006; Wetterich et al., 2008). We therefore attribute this ice wedge to the Holocene. A period of mild temperatures would increase the rate of biological respiration processes and the availability of organic matter. Note that the IW-26 samples plot on a slope of 6.63 ± 0.15 in the co-isotopic diagram of Fig. 3c, which deviates from the LMWL slope of 7.6 (Tiksi; Meyer, unpublished data). Paleoclimatic interpretation of the stable isotopes signature in ice wedges is usually challenged by the fact that phase changes such as evaporation or melting and refreezing are known to affect isotopic ratios through fractionation and therefore potentially alter the original paleoclimatic signature of the deposit. Refreezing processes will shift the δ values towards less negative values (e.g. max. +3 ‰ for $\delta^{18}O$ and +21 ‰ for

TCD
5, 3627–3660, 2011

δD in a single refreezing process) and will also decrease the slope of the δ^{18}O-δD co-isotopic relation (Souchez and Lorrain, 1991). This is described by the "freezing slope", which is expressed in the more general case of open systems as:

$$S = \frac{\alpha - 1}{\beta - 1} \cdot \frac{1000 + \delta_i \mathrm{D}}{1000 + \delta_i^{18}\mathrm{O}} \quad (1)$$

where $\alpha = 1.0208$ for deuterium; $\beta = 1.003$ for ^{18}O; δ_i = isotopic composition of the initial liquid.

Evaporation/sublimation processes or small scale refreezing processes (the calculated freezing slope would be 5.79 ± 0.02, using Eq. (1) and the mean IW-26 δ values) are 2 possible assumptions to explain the observed slope. Both alternatives would equally be favoured under relatively warm conditions, as hypothesised above.

The lower isotopic composition of IW-28 suggests a Pleistocene origin (δ^{18}O around −30 ‰). Although, the situation is probably more complex for the ISW-28/IW-28 case as displayed by a clear contrast in their d values, showing in both cases low variability, of ISW-28 (mean = 1.4 ‰) and IW-28 (mean = 7.5 ‰), for similar δD ranges (Fig. 3). There is a number of ways to explain low d in precipitation (and in the ice that evolves from it), that either belong to the "water cycle processes" or to the "in-situ post-deposition processes". Extensive work has been done dealing with the concept and use of the d in co-isotopic studies, especially in the field of deep ice core interpretation and the relation to temperature changes at precipitation sites and oceanic sources (Craig, 1961; Dansgaard, 1964; Johnsen et al., 1989; Jouzel and Merlivat, 1984; Jouzel et al., 2005a, b, 1982; Masson-Delmotte et al., 2005; Merlivat and Jouzel, 1979; Stenni et al., 2001, 2004; Vimeux et al., 2002, 1999; Yurtsever and Gat, 1981). It is commonly admitted that, although humidity and wind speed at the source also play a role, in most cases, the $\delta^{18}\mathrm{O}_{\mathrm{ice}}$ and $\delta\mathrm{D}_{\mathrm{ice}}$ primarily depends on the temperature at the site (T_{site}) and to a lesser extent on the temperature at the source (T_{source}). The reverse is true for the d in the ice. The latter is mainly driven by kinetic isotopic effects during evaporation at the oceanic source, and these will be enhanced for higher temperatures

TCD
5, 3627–3660, 2011

and lower relative humidity, increasing the d value (Masson-Delmotte et al., 2005). During the last glacial period (Dansgaard-Oeschger events), large topographic and atmospheric circulation changes are also responsible for an antiphase relationship between δ values (T_{site}) and d values (T_{source}). Indeed, during mild events, when Greenland was warmer (less negative δ's) and the sea ice extension lower, the moisture source was colder and therefore the d lower and vice-versa. This can explain the fact that the samples from these milder periods (less negative δD and δ^{18}O) are aligned on a line with slope close to 8, but with a d-intercept of +4 ‰ instead of +8 ‰ (e.g. Fig. 7 in Johnsen et al., 1989). The main source of the winter precipitation today is probably located in the Northern Atlantic (Kuznetsova, 1998; Rinke et al., 1999) and secondly potentially influenced by the Laptev Sea polynya (Meyer et al., 2002a). Pleistocene sources are more difficult to locate, nevertheless, Meyer et al. (2002a) have already discussed two possible hypotheses. The first one is the Atlantic with the latitudinal variation due to the ice area variation suggested by Johnsen and White (1989). The second one discusses about the potential variations of atmospheric moisture circulation due to the Eurasian ice sheet extension enabling a contribution from the Northern Pacific which is known to have a lower d. Meyer et al. (2010b) already have identified sources moisture variation during the Younger Dryas in Northern Alaska. In our case, the d shift between ISW-28 and IW-28 occurred during the Pleistocene, suggesting the contrasting δD-δ^{18}O signature of our coastal ice wedge ISW-28/IW-28 could represent a shift from a milder glacial period with a more proximal ocean source (due to a lesser sea ice cover) at a lower temperature (lower T_{source}, lower d values in ISW-28) to a colder glacial period with a more distal ocean source at a higher temperature (higher T_{source}, higher d value in IW-28). On the other hand, a radical modification of the source origin should be unlikely to explain this d shift without showing a clear gap in the isotopic profile. Climatic seasonal variations (temperature, precipitation, etc.) are also known to be able to disrupt d (Johnsen et al., 1989; Meyer et al., 2002a) but ice wedges are known to be built from the winter snow precipitation and the spring meltwater, therefore, it is delicate to discuss this hypothesis although earlier precipitations in Autumn with a lower d could

TCD
5, 3627–3660, 2011

be an explanation.

Post-depositional "in situ" phase changes could also be responsible for lowering the d values of the samples (Meyer et al., 2002a). Isotopic fractionation during ice wedge consolidation can be discarded according to Michel (1982), based upon the argument that freezing is generally too fast to allow for fractionation. However, conditions might be different for the formation of the "ribbon facies" of the ice-sand wedge. Figure 8 shows the effect of equilibrium fractionation during hypothetical 10 % refreezing (grey squares) of water resulting from the melting of each of the samples from IW-28 (black dots). The mean isotopic composition of the 10 % refrozen fraction was computed using the formulation in Souchez and Lorrain (1991) as in Eq. (2), with a frozen fraction $(K) = 0.10$.

$$\bar{\delta}_s = 10 \cdot (1000 + \delta_0) \cdot [(1.1 - K)^{\alpha} - (1 - K)^{\alpha}] - 1000 \quad (2)$$

where $\bar{\delta}_s = \delta$ value of refrozen samples; $\delta_0 = \delta$ value of water (melted IW-28 ice sample, no fractionation on melting (Moser and Stichler, 1980; Souchez and Lorrain, 1991)); K = frozen fraction; α = fractionation coefficient (1.0208 for deuterium and 1.003 for ^{18}O).

The modelled refrozen IW-28 samples using $K = 10$ reproduce the d of the ISW-28 samples and lie on the same co-isotopic line. They are however clearly offset towards less negative δ values. Experimental sublimation/evaporation processes of a snow pack have also been shown to shift the remaining reservoir towards less negative isotopic values with a slope that is less than 8 (Souchez and Lorrain, 1991, and references within). Submitting the IW-28 samples to such a fractionation process would also shift their d towards lower values. However, although they could reproduce the observed d values in ISW-28, both of these post-depositional processes would need to be occurring at a rigorous equivalent rate (e.g. 10 % refreezing, fixed evaporation percentage) for all samples to plot on a co-isotopic line as well defined as the one observed for the ISW-28 samples, with a slope close to 8. As a matter of fact, the very good alignment of all the ISW-28 samples on a line with slope 8.03 ($r^2 = 0.98$, with a fairly low range of the δ values) is in itself an argument to favour a "classical" Rayleigh-type "source to

TCD
5, 3627–3660, 2011

sink" fractionation history. This leaves us therefore with the first hypothesis of a major shift southward in the moisture source (higher d), as the ice wedge growth switches from ISW-28 to IW-28, across the transition zone. There is, however, an apparent discrepancy with similar cases in ice-core records (for example, shifts from mild to cold glacial periods as described in Fig. 7 of Johnsen et al., 1989), where an increase in the d value is always accompanied by a shift of both the δD and δ^{18}O values towards colder, more negative values (and vice-versa). This is less clear in the data of Fig. 3. Although the range of δ^{18}O values can reasonably be considered as "colder" in IW-28. This might be understandable for moderate coolings, since an increase in T_{source} will kinetically affect δ^{18}O more than δD. It seems also somewhat straightforward that the amplitude of changes in δ values between milder and colder event during the Pleistocene would be smaller closer to sea level than in the central part of the Greenland Ice Sheet. The relative contribution of T_{source} and T_{site} to the δ's signatures could also be different at coastal sites, but that would require model simulations for testing. Aside from the potential sources variation, the ice-sand wedge facies results from a local environment change with probably a thinner snow cover or an earlier cracks opening (before the snow cover presence) to enable the particles to be blown/entrained into the cracks. A very thin snow cover could change the local albedo by allowing the accumulation of particles on the snow, supporting more water streaming which should contribute to the formation of the "ribbon facies". A very thin snow cover might also suggest an important local role of sublimation and evaporation processes with potential post-depositional impact on the d-value, as suggested above. Although a constant sublimation rate needs to be invoked to explain the observed strict alignment of the samples along the co-isotopic slope, this hypothesis cannot be ruled out.

Regardless of the fact that both variation of local conditions and T_{source} modification might explain the d shift between ISW-28 and IW-28, in both cases the ISW-28 section reflects a climate characterized by milder temperatures, more important liquid water contribution to the ice genesis and a time period in the year with a very thin snow cover and access for the particles to the inner crack.

TCD
5, 3627–3660, 2011

6 Conclusions

We analyzed 2 ice wedges (IW-26 and IW-28) from a cliff located in Arctic Siberia, in order to understand the specific conditions of their formation process. Detailed crystallographic, gas content and composition, and water isotope analyses of the IW-26 and IW-28 ice wedges allowed us to shed more light on the processes involved in ice-wedge growth. Our multi-parametric approach suggest that water isotopes can be used locally as reliable climate indicators and that the studied ice wedges formed under different environmental conditions. The ice wedge IW-26 is found to have developed in a mild Holocene environment. Higher temperatures and higher meltwater infiltration resulted in enhanced recrystallization, larger crystal sizes, lower total gas content and favourable conditions for biological respiration, inducing relatively high CO_2 levels. Ice wedge ISW-28/IW-28 was initiated in a relatively mild Pleistocene environment, probably characterized by a moisture source with comparatively higher relative humidity, as revealed by the uniformly low *d* value in ISW-28. The local conditions at the time of formation were probably warmer than later on, favouring meltwater production in an environment characterized by periods of limited amount of snow and close proximity to a soil/sediment source, eventually further fostering melting through the albedo feedback. These conditions led to the typical "ribbon" layer texture. We interpret the low total gas content in the "ribbon" layers and the higher values in the surrounding equigranular texture as resulting from the freezing of a thin meltwater film running on the open frost crack of the ice wedge partially filled with snow. This heterogeneous medium, rich in organic matter, might have favoured the anaerobic microenvironmental conditions necessary to explain the maximum CH_4 levels in that unit. The analysis of *d* values further allowed constraining the local climatic conditions. As the climate started to cool, a transition occurred in the central part of the IW-28 ice wedge, as documented by the higher *d* values documenting in this part, suggesting a synchronous major change in the moisture source for the snow falls towards a more meridional ocean source. As suggested by several authors discussing the Greenland Pleistocene ice-core records,

TCD
5, 3627–3660, 2011

this might reflect the switch towards larger ice sheets and/or sea ice extents. These cooler conditions limited crystal size growth, total gas loss, biological respiration activities and CH_4 production, although the latter might also have been influenced by the unavailability of organic substrate. It should be noted that the system apparently never returned to milder climatic conditions before the ice wedge ceased being active, suggesting that its lifetime spanned a few thousand years at the most.

Acknowledgements. We thank all participants of the Russian-German expedition "Lena Anabar 2003". Sampling and analytical work in the AWI Potsdam laboratories was supported by Antje Eulenburg, Eileen Nebel, Ute Bastian and Lutz Schönicke. This study is part of the Russian-German cooperative scientific project "System Laptev Sea".

References

Barnola, J. M., Raynaud, D., Neftel, A., and Oeschger, H.: Comparison of CO_2 measurements by two laboratories on air from bubbles in polar ice, Nature, 303, 410–413, 1983.

Black, R. F.: Permafrost – A review, Bulletin of the Geological Society of America, 65, 839–856, 1954.

Black, R. F.: Les coins de glace et le gel permanent dans le Nord de l'Alaska, Annales de Géographie, 72, 257–271, 1963.

Black, R. F.: Features indicative of permafrost, Annual Reviews Inc. Provided by the NASA Astrophysics Data System, 75–94, 1976.

Black, R. F.: Fabrics of ice wedges in central Alaska, in Third International Conference on Permafrost, pp. 247–253, National Research Council of Canada, 1978.

Blunier, T., Chappellaz, J. A., Schwander, J., Barnola, J.-M., Desperts, T., Stauffer, B., and Raynaud, D.: Atmospheric methane record from a Greenland ice core over the last 1000 years, Geophys. Res. Lett., 20, 2219–2222, 1993.

Bobrov, A. A., Muller, S., Chizhikova, N. A., Schirrmeister, L., and Andreev, A. A.: Testate amoebae in late quaternary sediments of the Cape Mamontov Klyk (Yakutia), Biol. Bull, 36, 363–372, 2009.

Brouchkov, A. and Fukuda, M.: Preliminary Measurements on Methane Content in Permafrost,

TCD

5, 3627–3660, 2011

Central Yakutia, and some Experimental Data, Permafrost and Periglacial Processes, 13, 187–197, 2002.
Brown, J. and Romanovsky, V. E.: Report from the International Permafrost Association: state of permafrost in the first decade of the 21st century, Permafrost and Periglacial Processes, 19, 255–260, 2008.
Cardyn, R., Clark, I. D., Lacelle, D., Lauriol, B., Zdanowicz, C., and Calmels, F.: Molar gas ratios of air entrapped in ice: A new tool to determine the origin of relict massive ground ice bodies in permafrost, Quaternary Res., 68, 239–248, 2007.
Corte, A. E.: Relationship between four ground patterns, structure of the active layer and type and distribution of ice in permafrost Thule, Groenland, US Army Cold Regions Research and Engineering Laboratory, Corps of Engineers, Research Report, 88, Hanover, 79 p., February 1962.
Craig, H.: Isotopic variations in meteoric waters, Science, 133, 1702–1703, 1961.
Dansgaard, W.: Stable isotopes in precipitation, Tellus, 16, 436–468, 1964.
Dereviagin, A. Y., Meyer, H., Chizhov, A. B., Hubberten, H.-W., and Simonov, E. F.: New data on the isotopic composition and evolution of modern ice wedges in the Laptev Sea region, Polarforschung, 70, 27–35, 2002.
Gell, W. A.: Underground Ice in Permafrost, Mackenzie Delta-Tuktoaktuk, N.W.T,, 1976.
Gell, W. A.: Fabrics of icing-mound and pingo ice in permafrost, J. Glaciol., 20, 563–569, 1978a.
Gell, W. A.: Ice-wedge ice, Mackenzie delta-Tuktoyaktuk peninsula area, N.W.T., Canada, J. Glaciol., 20, 555–562, 1978b.
IPCC: Climate change 2007: The physical Science Basis, Cambridge University Press., 2007.
Jacka, T. H.: Laboratory studies on relationships between ice crystal size and flow rate, Cold Regions Science and Technology, 10, 31–42, 1984.
Johnsen, S. J., Dansgaard, W., and White, J. W. C.: The origin of Arctic precipitation under present and glacial conditions, Tellus, 41B, 452–468, 1989.
Jouzel, J. and Merlivat, L.: Deuterium and oxygen 18 in precipitation: modeling of the isotopic effects during snow formation, J. Geophys. Res., 89, 11749–11757, 1984.
Jouzel, J., Merlivat, L., and Lorius, C.: Deuterium excess in an East Antarctic ice core suggests higher relative humidity at the oceanic surface during the last glacial maximum, Nature, 299, 688–691, 1982.
Jouzel, J., Masson-Delmotte, V., Stiévenard, M., Landais, A., Vimeux, F., Johnsen, S. J., Svein-

TCD
5, 3627–3660, 2011

bjornsdottir, A., and White, J. W. C.: Rapid deuterium-excess changes in Greenland ice cores?: a link between the ocean and the atmosphere, C. R. Géoscience, 337, 957–969, 2005a.
Jouzel, J., Stiévenard, M., Johnsen, S. J., Landais, A., Masson-Delmotte, V., Sveinbjornsdottir, A., Vimeux, F., von Grafenstein, U. and White, J. W. C.: The GRIP deuterium-excess record, Quaternary Sci. Rev., 26, 1–17, 2005b.
Killawee, J. A., Fairchild, I. J., Tison, J.-L., Janssens, L., and Lorrain, R.: Segregation of solutes and gases in experimental freezing of dilute solutions: Implications for natural glacial systems, Geochemica et Cosmochimica Acta, 62, 3637–3655, 1998.
Knight, P. G.: Glaciers, Stanley Thornes Ltd., 1999.
Kolchugina, T. and Vinson, T. S.: Climate warming and the carbon cycle in the permafrost zone of the former Soviet Union, Permafrost and periglagial process, 4, 149–163, 1993.
Kuznetsova, L. P.: Atmospheric moisture content and transfer over the territory of the former USSR, in: Second International Workshop on Energy and Water Cycle in GAMESiberia, 1997, edited by: Ohata, T. and Hiyama, T., Research Report of IHAS. Institute for Hydrospheric-Atmospheric Sciences, Nagoya University: Nagoya, Japan;, 145–151, 1998.
Lambert, G., Chappellaz, J., Foucher, J.-P., and Ramstein, G.: Le méthane et le destin de la Terre. Les hydrates de méthane: rêve ou cauchemar?, EDP Sciences, 168 p., ISBN: 2-86883-829-4, 2006.
Langway, C. C. J.: Ice fabrics and the universal stage, SIPRE Technical Report, 62, 1958.
Lauriol, B., Duchesne, C., and Clark, I. D.: Systématique du remplissage en Eau des Fentes de Gel: les Résultats d'une étude Oxygène-18 et Deutérium, Permafrost and Periglacial Processes, 6, 47–55, 1995.
Lawson, W.: Environmental Conditions, Ice Facies and Glacier Behaviour, in: Glacier Science and Environmental Change, edited by: Knight, P. G., pp. 319–328, Blackwell, 2007.
Martinerie, P., Raynaud, D., Etheridge, D. M., Barnola, J. M., and Mazaudier, D.: Physical and climatic parameters which influence the air content in polar ice, Earth Planet. Sci. Lett., 112, 1–13, 1992.
Martinerie, P., Lipenkov, V. Y., Raynaud, D., Chappellaz, J., Barkov, N. I., and Lorius, C.: Air content paleo record in the Vostok ice core (Antarctica): A mixed record of climatic and glaciological parameters, J. Geophys. Res., 99, 10565–10576, 1994.
Masson-Delmotte, V., Jouzel, J., Landais, A., Stievenard, M., Johnsen, S. J., White, J. W. C., Werner, M., Sveinbjornsdottir, A., and Fuhrer, K.: GRIP Deuterium Excess Reveals Rapid

TCD
5, 3627–3660, 2011

and Orbital-Scale Changes in Greenland Moisture Origin, Science, 309, 118–121, 2005.
Merlivat, L. and Jouzel, J.: Global climatic interpretation of the deuterium-oxygen 18 relationship for precipitation., J. Geophys. Res., 84, 5029–5033, 1979.
Meyer, H., Schönicke, L., Wand, U., Hubberten, H.-W., and Friedrichsen, H.: Isotope studies of hydrogen and oxygen in ground ice?? Experiences with the equilibration technique, Isotopes in Environmental and Health Studies, 36, 133–149, 2000.
Meyer, H., Dereviagin, A. Y., Siegert, C., and Hubberten, H.-W.: Paleoclimate studies on Bykovsky Peninsula, North Siberia – hydrogen and oxygen isotopes in ground ice, Polarforschung, 70, 37–51, 2002a.
Meyer, H., Dereviagin, A., Siegert, C., Schirrmeister, L., and Hubberten, H.-W.: Palaeoclimate Reconstruction on Big Lyakhovsky Island, North Siberia – Hydrogen and Oxygen Isotopes in Ice Wedges, Permafrost and Periglacial Processes, 13, 91–105, 2002b.
Meyer, H., Schirrmeister, L., Andreev, A., Wagner, D., Hubberten, H.-W., Yoshikawa, K., Bobrov, A., Wetterich, S., Opel, T., Kandiano, E., and Brown, J.: Lateglacial and Holocene isotopic and environmental history of northern coastal Alaska – Results from a buried ice-wedge system at Barrow, Quaternary Sci. Rev., 29, 3720–3735, doi:10.1016/j.quascirev.2010.08.005, 2010a.
Meyer, H., Schirrmeister, L., Yoshikawa, K., Opel, T., Wetterich, S., Hubberten, H.-W., and Brown, J.: Permafrost evidence for severe winter cooling during the Younger Dryas in northern Alaska, Geophys. Res. Lett., 37, L03501, doi:10.1029/2009GL041013, 2010b.
Michel, F. A.: Isotope investigations of permafrost waters in northern Canada, University of Waterloo, Ontario, Canada, Dept. of Earth Sciences., 1982.
Moser, H. and Stichler, W.: Environmental isotopes in ice and snow, in: Handbook of Environmental Isotope Geochemistry, the terrestrial environment, 1A, edited by: Fritz, P. and Fontes, J., pp. 141–178, Elsevier, Amsterdam., 1980.
Nelson, F. E. and Anisimov, O. A.: Permafrost zonation in Russia under anthropogenic climatic change, Permafrost and periglagial process, 4, 137–148, 1993.
Paterson, W. S. B.: The physics of glaciers, third edition, Butterworth-Heinemann, Oxford., 1994.
Pickering, F. B.: The basis of Quantificative Metallography., Metals and Metallurgy Trust., 1976.
Raffi, R., Stenni, B., Flora, O., Polesello, S., and Camusso, M.: Growth processes of an inland Antarctic ice wedge, Mesa Range, northern Victoria Land, Ann. Glaciol., 39, 379–385, 2004.
Raynaud, D., Delmas, D., Ascencio, J. M., and Legrand, M.: Gas extraction from polar ice

TCD
5, 3627–3660, 2011

cores: a critical issue for studying the evolution of atmospheric CO2 and ice-sheet surface elevation, Ann. Glaciol., 3, 265–268, 1982.
Raynaud, D., Chapellaz, J., Barnola, J. M., Korotkevich, Y., and Lorius, C.: Climatic and CH4 cycle implications of glacial-interglacial CH4 change in the Vostok ice core, Nature, 333, 655–657, 1988.
Rinke, A., Dethloff, K., Spekat, A., Enke, W., and Hesselbjerg Christensen, J.: High resolution climate simulations over the Arctic, Polar Research; Vol 18, No 2 (1999): Special issue: Proceedings of the International Symposium on Polar Aspects of Global Change [online], available from: http://www.polarresearch.net/index.php/polar/article/view/6567, 1999.
Samyn, D., Fitzsimons, S., and Lorrain, R.: Strain-induced phase changes within cold basal ice from Taylor Glacier, Antarctica, indicated by textural and gas analyses, J. Glaciol., 51, 611–619, 2005.
Schirrmeister, L., Grosse, G., Kunitsky, V., Magens, D., Meyer, H., Dereviagin, A., Kuznetsova, T., Andreev, A., Babiy, O., Kienast, F., Grigoriev, M., Overduin, P. P., and Preusser, F.: Periglacial landscape evolution and environmental changes of Arctic lowland areas for the last 60,000 years (Western Laptev Sea coast, Cape Mamontov Klyk), POLAR RESEARCH, 27, 249–272, 2008.
Shumskii, P. A.: Principles of structural glaciology – The petrography of fresh-water ice as a method of glaciological investigation, Dover Publications, Inc., New York., 1964.
Souchez, R. and Lorrain, R.: Ice Composition and Glacier Dynamics, Springer-Verlag, 1991.
Souchez, R., Janssens, L., Lemmens, M., and Stauffer, B.: Very low oxygen concentration in basal ice from Summit, Central Greenland, Geophys. Res. Lett., 22, 2001–2004, 1995a.
Souchez, R., Jouzel, J., Landais, A., Chapellaz, J., Lorrain, R., and Tison, J.-L.: Gas isotopes in ice reveal a vegetated central Greenland during ice sheet invasion, Geophys. Res. Lett., 33, L24503, doi:10.1029/2006GL028424, 2006.
Souchez, R., Lemmens, M., and Chapellaz, J.: Flow-induced mixing in the GRIP basal ice deduced from the CO2 and CH4 records, Geophys. Res. Lett., 22, 41–44, 1995b.
Stenni, B., Masson-Delmotte, V., Johnsen, S., Jouzel, J., Longinelli, A., Monnin, E., Röthlisberger, R., and Selmo, E.: An Oceanic Cold Reversal During the Last Deglaciation, Science, 293, 2074–2077, 2001.
Stenni, B., Jouzel, J., Masson-Delmotte, V., Röthlisberger, R., Castellano, E., Cattani, O., Falourd, S., Johnsen, S. J., Longinelli, A., Sachs, J. P., Selmo, E., Souchez, R., Steffensen, J. P., and Udisti, R.: A late-glacial high-resolution site and source temperature record de-

TCD
5, 3627–3660, 2011

rived from the EPICA Dome C isotope records (East Antarctica), Earth Planet. Sci. Lett., 217, 183–195, 2004.
Tison, J.-L.: Diamond-wire saw cutting technique for investigating textures and fabrics of debris-laden ice and brittle ice, J. Glaciol., 40, 410–414, 1994.
Tison, J.-L., Souchez, R., Wolff, E. W., Moore, J. C., Legrand, M. R., and de Angelis, M.: Is a periglacial biota responsible for enhanced dielectric response in basal ice from the Greenland Ice Core Project ice core??, J. Geophys. Res., 103, 18885–18894, 1998.
Vaikmäe, R.: Oxygen isotopes in permafrost and ground ice – a new tool for paleoclimatic investigations, Leipzig, 1989.
Vasil'chuk, Y. K. and Vasil'chuk, A. C.: Oxygen-isotope and C14 data associated with Late Pleistocene syngenetic ice-wedges in mountains of Magadan region, Siberia, Permafrost and Periglacial Processes, 9, 177–183, 1998.
Vimeux, F., Masson-Delmotte, V., Jouzel, J., Stiévenard, M., and Petit, J. R.: Glacial-interglacial changes in ocean surface conditions in the southern Hemisphere, Nature, 398, 410–413, 1999.
Vimeux, F., Cuffey, K., and Jouzel, J.: New insights into Southern Hemisphere temperature changes from Vostok ice cores using deuterium excess correction over the Last 420,000 Years, Earth Planet. Sci. Lett., 203, 829–843, 2002.
Wagner, D. and Liebner, S.: Global warming and carbon dynamics in permafrost soils: Methane production and oxidation, in: Permafrost Soils, edited by: Margesin, R., pp. 219–236, Springer Berlin Heidelberg, 2009.
Yershov, E. D.: Geokryologija SSSR (Geocryology of the USSR), Nedra, Moscow., 1989.
Yurtsever, Y. and Gat, J. R.: Atmospheric waters, in: Stable Isotope Hydrology: Deuterium and Oxygen in Water Cycle, T. Rep., pp. 103–145, IAEA, Vienna., 1981.
Zeebe, R. E. and Wolf-Gladrow, D.: CO_2 in Seawater: Equilibrium, Kinetics, Isotopes, 65, Elsevier, 2001.

TCD
5, 3627–3660, 2011

Table 1. Summary of gas results and comparison with the atmosphere and the meteoric ice. Values separated with – are the minimum and the maximum, the number between ( ) corresponds to the mean.

	Total gas content ($ml\,kg^{-1}$)	CO_2 (ppmV)	CH_4 (ppmV)	O_2 (%)	N_2 (%)
IW-26	10–36 (27)	35 000–110 000 (62 000)	0.5–1.6 (1)	5–13 (10)	77–86 (82)
ISW-28	11–42 (25)	860–7000 (3000)	41–72 (55)	10–21 (15)	78–89 (85)
IW-28	27–50 (45)	10 000–48 000 (25 000)	7–10 (8)	10–15 (12)	82–89 (86)
Atmosphere (pre-industrial)	–	280	0.6	21	78
Atmosphere (present)	–	380	1.75	21	78
Meteoric ice	75–140*	–	–	–	–

* Martinerie et al. (1992)

TCD
5, 3627–3660, 2011

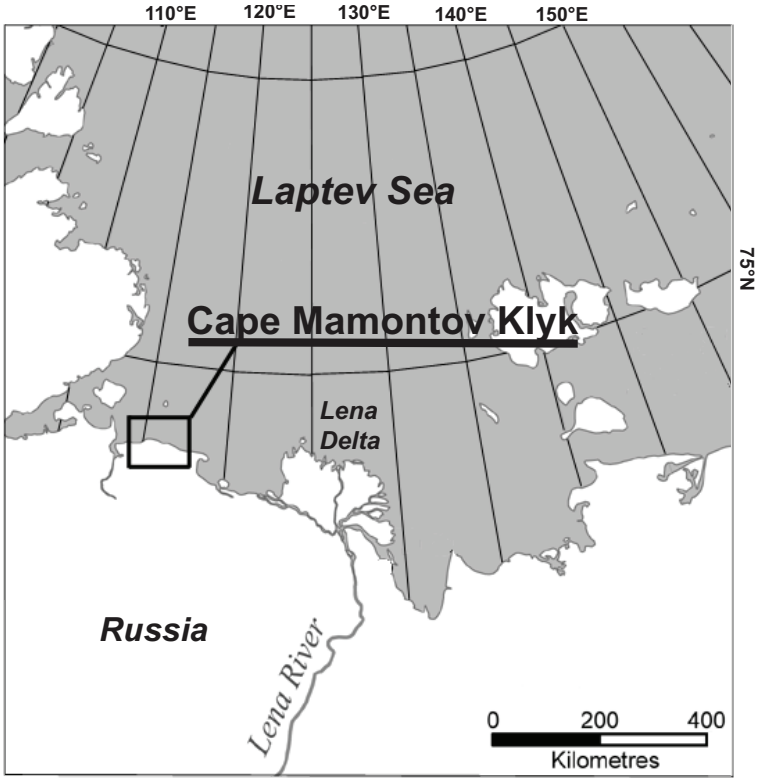

Fig. 1. Location of the Cape Mamontov Klyk sampling site in Arctic Siberia.

TCD
5, 3627–3660, 2011

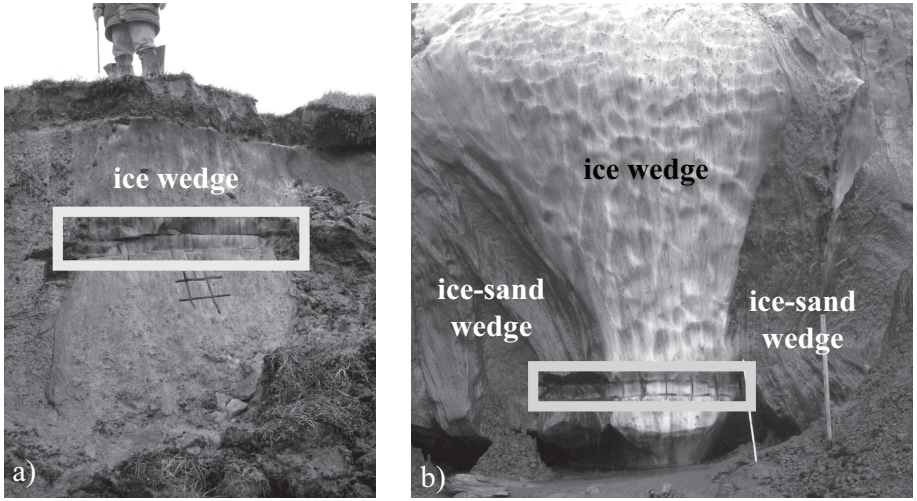

Fig. 2. General settings of ice wedges 26 (IW-26, left) and 28 (IW-28, right). The sampling areas are outlined with black boxes. Note that IW-28 was sampled in both the ice-sand wedge (ISW-28, left of box) and in the ice wedge itself (IW-28, right of box).

TCD
5, 3627–3660, 2011

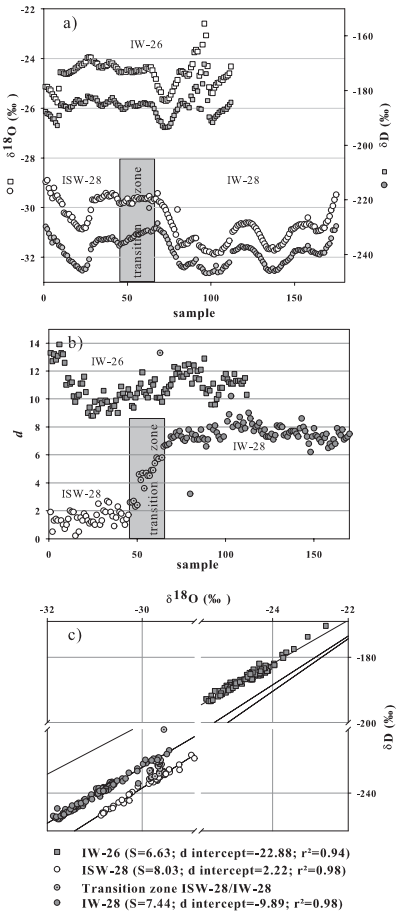

Fig. 3. Isotopic data for the two ice wedges: **(a)** δ^{18}O and δD profiles, **(b)** d and **(c)** δ^{18}O-δD relationship. Numbers on the x-coordinate of **(a)** and **(b)** refer to ice sample ordering, increasing from left to right, in the outcrop.

TCD
5, 3627–3660, 2011

Stable isotope and gas properties of two ice wedges from Cape Mamontov Klyk

T. Boereboom et al.

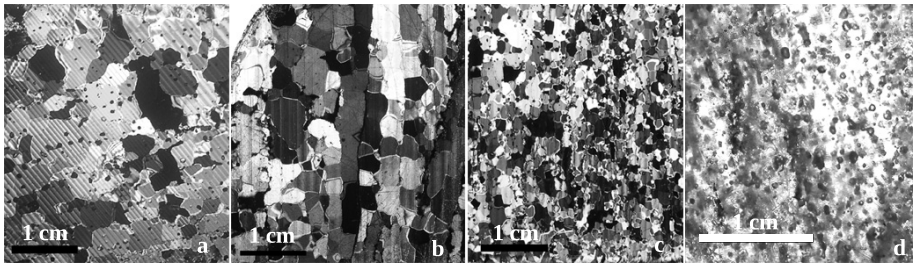

Fig. 4. Textural properties of the ice wedges. **(a)** IW-26, **(b)** ISW-28 (ice-sand wedge), the left part of ice wedge 28 with debris sub vertical layers (note the crystal elongation along the foliation), **(c)** IW-28, clean ice in the central part of ice wedge 28 and **(d)** thick section photograph of ice from IW-28 in transmitted light allowing the bubble content observation.

TCD
5, 3627–3660, 2011

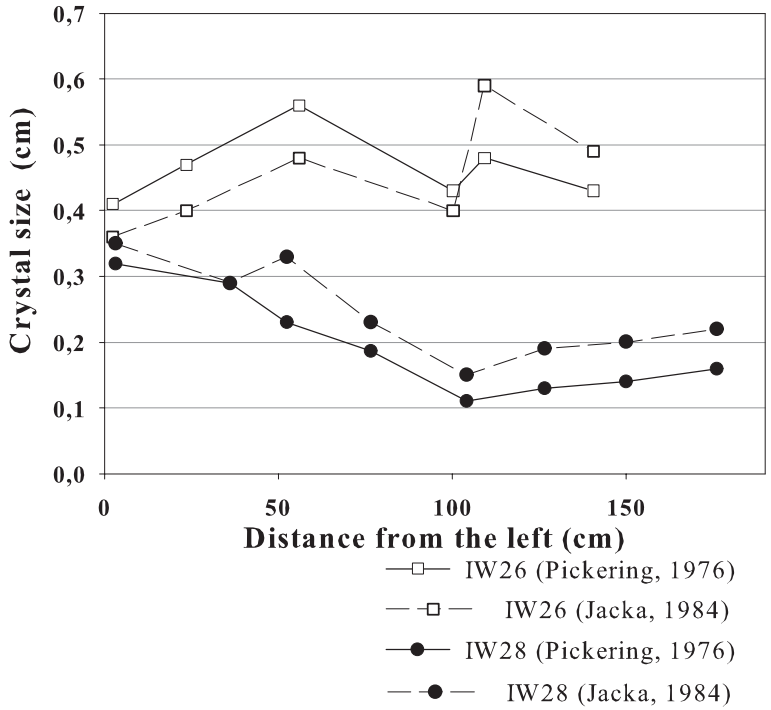

Fig. 5. Crystals size measurements using the two techniques described in the "sampling and analytical methods" section.

TCD
5, 3627–3660, 2011

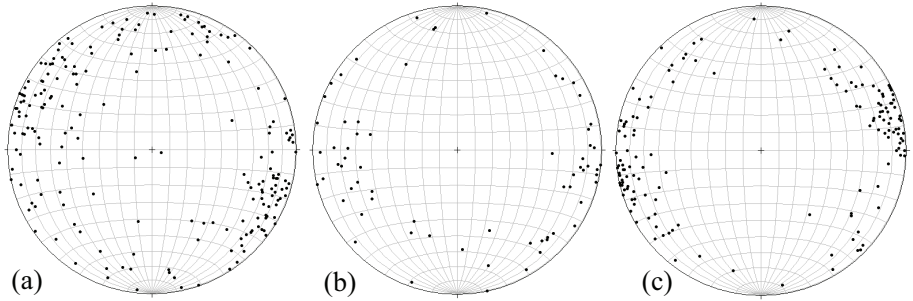

Fig. 6. Schmidt equal-area diagrams for the c-axes of horizontal thin sections. **(a)** a total of six thin sections from IW-26 ($n = 199$), **(b)** a total of two thin sections from ISW-28 ($n = 70$), **(c)** a total of five thin sections from IW-28 ($n = 150$).

TCD
5, 3627–3660, 2011

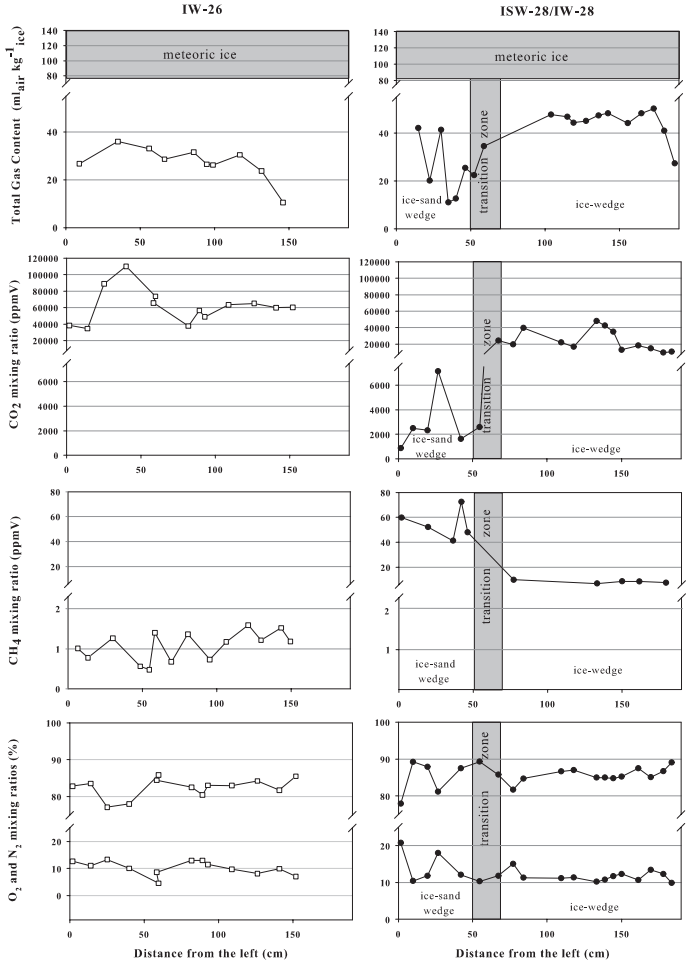

Fig. 7. Gas properties of ice wedges IW-26 (left) and ISW-28/IW-28 (right).

TCD
5, 3627–3660, 2011

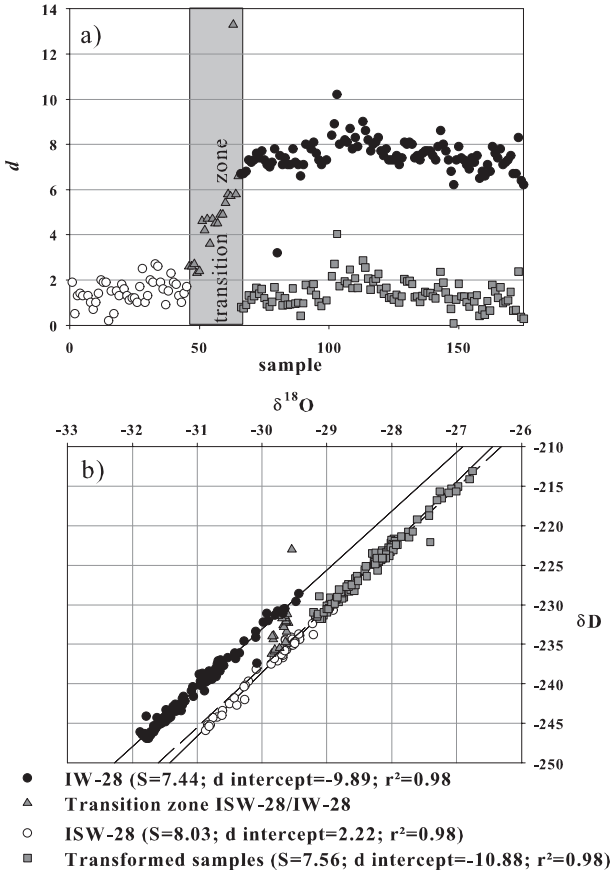

Fig. 8. *d* **(a)** and co-isotopic plots **(b)** of observed data for ISW-28 (open circles) and IW-28 (black dots) compared to a simulation (grey squares) on the effect of hypothetical equilibrium refreezing of 10 % of melted fraction in IW-28 sample, using Eq. (1) (see text for details).

TCD
5, 3627–3660, 2011